Seventh International Conference on CFD in the Minerals and Process Industries
CSIRO, Melbourne, Australia
9-11 December 2009

THE EFFECTS OF VORTEX BREAKDOWN BUBBLES ON THE MIXING ENVIRONMENT INSIDE A BASE DRIVEN BIOREACTOR

Stuart J. COGAN[1*], Gregory J. SHEARD[1] and Kris RYAN[1]

[1] Fluids Laboratory for Aeronautical and Industrial Research (FLAIR), Department of Mechanical Engineering, Monash University, Victoria 3800, AUSTRALIA
*Corresponding author, E-mail address: stuart.cogan@eng.monash.edu.au

ABSTRACT

The bubble-type vortex breakdown that occurs on the axis of a confined vortex, for example inside a cylinder with flow driven by rotation of the base, has applications in mixing. This configuration has well defined boundary conditions that are easily manipulated experimentally as well as numerically, and has traditionally been of interest to researchers in the fields of aircraft dynamics and stability theory or dynamical systems. Recently, interest in the vortex breakdown flow that develops on the axis in open cylindrical vessels has grown in relation to its application to mixing. In particular, it may provide a means for modulating certain fluid dynamic parameters of importance in mixing applications in fields including bioengineering. In most cell and tissue culture applications (be they suspension or scaffold based), a laminar, low-shear environment with high oxygen and nutrient density is desired. Therefore, levels of turbulence, shear stress, and the mass transport properties of mixing vessels are of great import. We investigate the vortex breakdown flow in the presence of immersed bodies and report on the flow states, and fluid dynamic properties achievable under different operating conditions, in a novel mixing vessel for use in scaffold-based tissue engineering.

NOMENCLATURE

a	maximum scaffold half height
b	scaffold radius
H	bioreactor cylinder height
P	kinematic pressure
p	pressure
R	bioreactor cylinder radius
Re	Reynolds number
t	time
$\mathbf{u}$	velocity vector
u_r	radial velocity
u_z	axial velocity
u_θ	azimuthal velocity
Γ	cylinder aspect ratio
ρ	density
υ	kinematic viscosity
Ω	cylinder base angular velocity

INTRODUCTION

A bioreactor can be described as any vessel that combines cells, tissue or other organic matter, together with chemicals and nutrients, commonly known as *culture medium*, in a way such as to stimulate the reproduction and proliferation of said organic matter (Darling *et al*., 2003). Generally they can be split into two classes, *suspension based* and *scaffold based*, where the organic matter being cultured is either suspended in the medium and harvested as a batch of cells and cell aggregates, or anchored to the surface and interior of a porous scaffold (either fixed in space or suspended in the fluid medium) and harvested as a single construct, respectively. This investigation will deal only with scaffold based tissue culture applications.

Over the past two decades numerous prototype bioreactors have been suggested for the production of cartilage, bone and other tissue types. These include simple petri-dish reactors which provide a static culture environment (Vunjak-Novakovic *et al*., 1996), mixed flasks which provide a well mixed turbulent environment (Vunjak-Novakovic *et al*., 1996), horizontal-axis rotating drum type reactors that provide a laminar mixing environment (Begley and Kleis, 2000), and perfusion reactors where culture medium is perfused through the scaffold (Niklason *et al*., 1999). These configurations are the most common types that have been investigated and the results from numerous physical tests of these reactors with real tissue samples have shown that further design improvements are required before functional tissue equivalents can be created *in vitro* (Vunjak-Novakovic, 2003). The most common deficiencies are: 1) lack of a spatially homogenous flow field in the vicinity of the scaffold construct causing non-uniform levels of nutrient absorption and physical force exposure over the surface area; 2) levels of physical forces that are inappropriate (non-physical) to the tissue being grown, this usually manifests as an undesirably high level of shear stress, but can also be insufficient levels of shear, as well as too much or too little compressive force; 3) insufficient mass transport through the flow field brought about by poor mixing mechanisms; and 4) the presence of turbulent structures in the flow which are non-physiological and can be seminal to the first three issues above.

It is with the above ideas in mind that we proceed with the investigation of the flow environment inside a novel bioreactor design for scaffold based tissue culture. We investigate the flow inside an open circular cylinder, driven by the constant rotation of the cylinder base, beginning with the analysis of the flow and the development of vortex breakdown bubbles (VBBs), in the absence of immersed bodies, before considering the effect of different shaped bodies located in the flow on the cylinder axis, in the vicinity of the bubbles. Besides the well defined boundary conditions and presence of the free surface to facilitate oxygen exchange, it is the development of these VBBs that makes this apparatus unique among possible candidates for bioreactors. It has been postulated (Dusting *et al*., 2006) that the slowly recirculating fluid inside the VBB may provide an

improved, low shear, homogenous and highly controllable environment for scaffold culture. Numerous other advantages include the isolation of the fluid in the VBB with respect to the bulk flow, possibly allowing for direct injection of fresh nutrients and/or extraction of waste products, to and from the growing construct, respectively, as well as the multitude of sizes, shapes and interior flow velocities observed for VBB at different Reynolds numbers. Here we conduct a more general investigation into the interaction between the construct and the bubble, and the effect of both bubble presence and construct shape on the forces seen by the construct surface, for a construct located in a fixed position in the vicinity of, but *outside*, the VBB.

MODEL DESCRIPTION

Physical Model

The physical system being investigated is shown schematically in figure 1, along with the base mesh used for the simulations of the cases with no immersed body present. The system consists of a circular cylinder of height H and radius R, with the height-to-radius ratio $\Gamma=H/R$ fixed at $\Gamma=$ 1.5. The top of the cylinder is open exposing the surface of the fluid of kinematic viscosity υ to the atmosphere and allowing for the insertion and suspension of an object representing a scaffold construct. Typically these constructs are supported by thin needles of negligible diameter that have been shown to not significantly affect the flow when located on the cylinder axis (Hussain *et al*., 2003). Thus, we neglect the presence of the supporting needles. The free surface is modelled as flat and stress-free throughout our investigation, an accurate assumption for cylinders with $\Gamma>1$ (Lopez *et al.*, 2004). The base rotates at a constant angular velocity Ω, driving the flow and facilitating the mixing. The scaffold profile under investigation takes one of two forms being either an axisymmetric disk or an ellipsoid (also axisymmetric), with axial dimension a and radial dimension b, with its centre located midway up the cylinder axis. Scaffold dimensions where determined such that the ratio of vessel volume to scaffold volume was1000:1 and the ratio of scaffold radius to scaffold half height was 10:1, chosen to be consistent with numerous cases from the tissue engineering literature. Base meshes employed for both construct geometries are shown in figure 2. The Reynolds number for the system is defined as

$$\mathrm{Re}=\frac{R^2\Omega}{\nu} \tag{1}$$

and we consider a range of $600\leq Re\leq 2100$. This represents a range of Re corresponding to conditions (Wootton and Ku, 1999), and characteristic of those encountered in the bioreactor literature (Dusting *et al*., 2006). We truncate our analysis at Re=2100 due to early indications from a stability analysis (not reported here) that the assumption of axisymmetry in the velocity field loses validity beyond this Re.

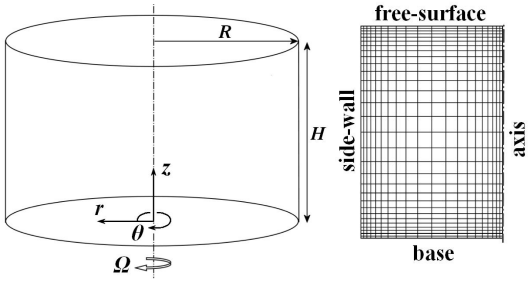

(a) (b)

Figure 1: Schematic diagram of geometry with no immersed body: (a) the bioreactor cylinder showing defining parameters and coordinate system, and (b) base mesh showing macro elements and boundary conditions.

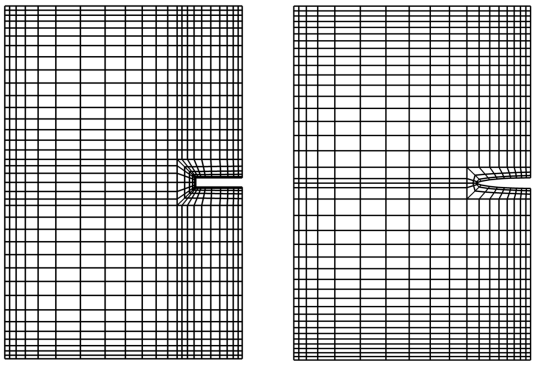

(a) (b)

Figure 2: Base meshes showing macro elements for (a) the disk scaffold geometry, and (b) the ellipsoid geometry.

Numerical Details

The fluid in the cylinder is assumed incompressible and Newtonian throughout, thus conservation of momentum and mass for the fluid yield

$$\frac{\partial \mathbf{u}}{\partial t}+(\mathbf{u}\cdot\nabla)\mathbf{u}=-\nabla P+\nu\nabla^2\mathbf{u} \tag{2}$$

$$\nabla\cdot\mathbf{u}=0 \tag{3}$$

where $\mathbf{u}$ represents the vector velocity field, t is time and $P=p/\rho$ is the kinematic scalar pressure field where p is the scalar pressure field and ρ is density. Simulations are performed using an in-house package that utilises a nodal spectral element method to discretise the flow field in the meridional (r, z) semi-plane. Within each macro element flow variables are computed at Gauss-Legendre-Lobatto (GLL) quadrature points. The combination of high order polynomial shape functions used to compute flow variables over the GLL quadrature points on a sparse mesh and the governing equations being solved in weak form, following application of the Galerkin method of weighted residuals, allows for accurate simulations achieving spectral convergence. This approach was recently employed for the case of flow past spheres moving in a circular tube (Sheard and Ryan, 2007). Equations (2) and (3) are integrated forward in time using an operator-splitting technique and a third-order accurate backwards-multistep scheme. Details can be found in Karniadakis *et al*. (1991).

The boundary conditions employed for the empty cylinder cases are: no-slip at the vertical sidewalls $(u_r, u_z, u_\theta) = 0$, a steady single component velocity $(u_r, u_z, u_\theta) = (0,0,r\Omega)$ along the base, and a flat stress-free constraint on the surface, achieved by a symmetry condition $(u_\theta, \partial u_{r,z}, \partial u_{z,z}, \partial u_{\theta,z}) = 0$. As the flow is known to be axisymmetric over the range of Reynolds numbers considered, only one half of the meridional plane is modelled, with a symmetry condition at the axis and all azimuthal derivatives set to zero $(\partial_\theta = 0)$ throughout the domain. The boundary conditions remain the same when an immersed body is present on the axis, with the addition of a no-slip condition applied to the boundary representing the construct surface. The initial condition for the flow field is zero velocity throughout the domain and the base is set impulsively into motion.

Final spatial resolution is determined at run time by specifying the order of interpolating polynomial within each macro element. For all the results reported here, simulations were performed using 9th order polynomial interpolants, over base grids containing 600, 882 and 748 macro elements for the cases shown in figures 1b, 2a and 2b, respectively. These combinations were found to found to produce results accurate to 0.1% of very highly resolved reference cases.

RESULTS AND DISCUSSION

Base Flow without Immersed Body

For the empty vessel, rotation of the base at constant angular velocity Ω drives the swirling flow by imparting angular momentum to the fluid adjacent to it. The fluid in the boundary layer that forms on the disk (known as an Ekman layer) is dragged by viscous stresses in the azimuthal direction (Healey, 2007), creating the primary swirling flow. The flow in the boundary layer also has a radial flow component which transports angular momentum towards the cylinder outer walls where it is turned in the positive axial direction. The fluid then flows up towards the surface until Froude number constraints at the surface force the fluid to return to the inner part of the cylinder where, upon colliding with the fluid returning from other parts of the perimeter, it is turned in the negative axial direction forming the much studied secondary over-turning meridional flow. This basic state is shown in figure 3a for Re = 600, where the left hand side of the meridional plane is shown, such that the right hand side of the figure represents the cylinder axis. As Reynolds number is increased, fluid with more and more angular momentum is forced to smaller radii by the overturning flow, and the streamlines in the meridional plane are forced to gradually redistribute in such a way as to satisfy conservation of momentum. At some point near the axis a localised region of azimuthal vorticity develops, with opposite sign to that of the bulk flow, leading to an induced velocity in the positive axial direction. This induced velocity opposes the flow returning to the cylinder base down the central vortex core and a stagnation point forms on the axis where the magnitude of the negative axial velocity shrinks to zero.

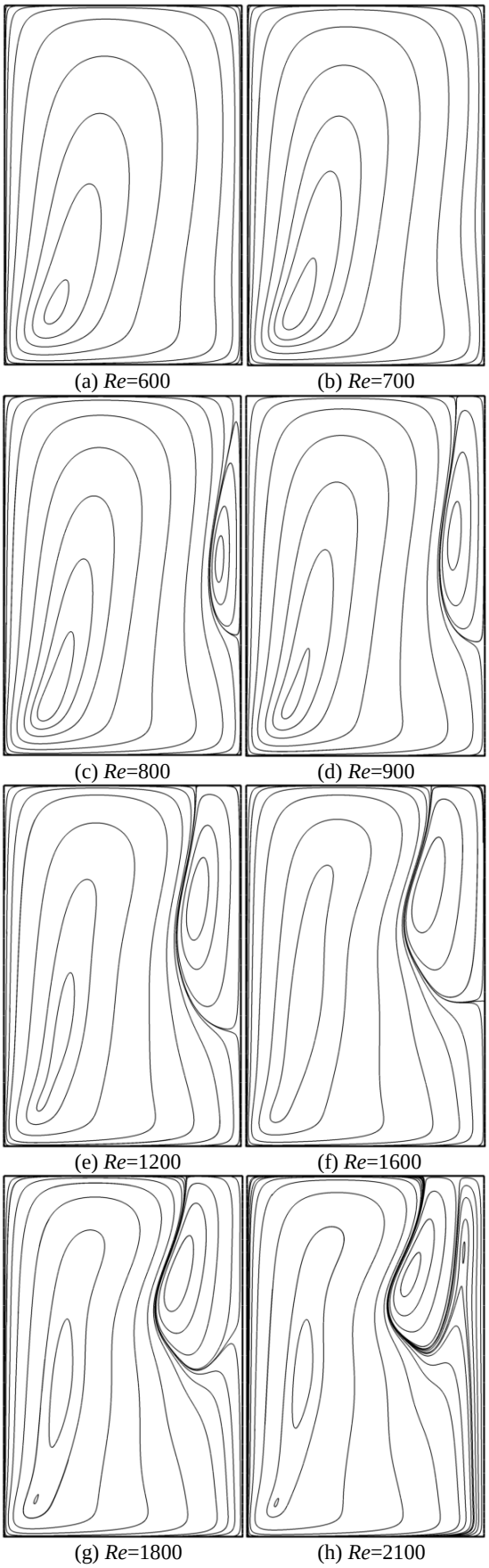

(a) *Re*=600 (b) *Re*=700

(c) *Re*=800 (d) *Re*=900

(e) *Re*=1200 (f) *Re*=1600

(g) *Re*=1800 (h) *Re*=2100

Figure 3: Streamlines in the left meridional plane detailing the evolution of the vortex breakdown flow with Reynolds number, cases as labelled.

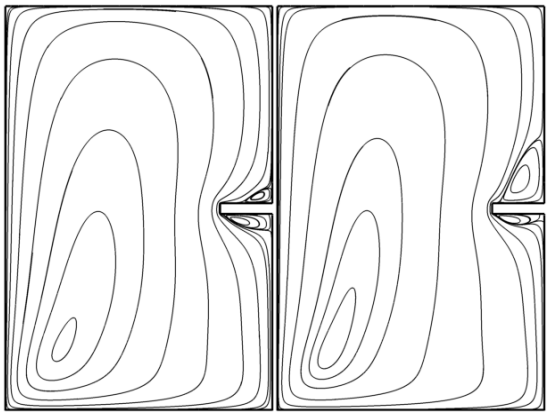

(a) *Re*=600 (b) *Re*=700

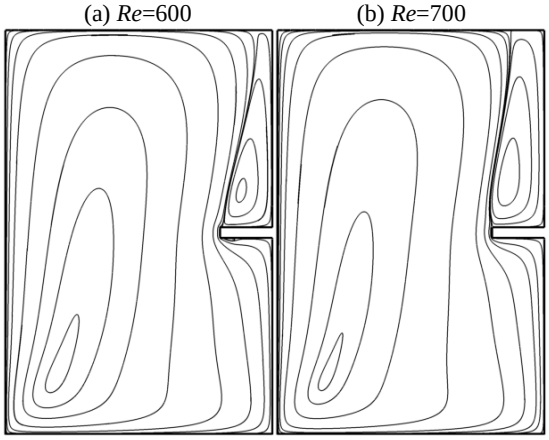

(c) *Re*=800 (d) *Re*=900

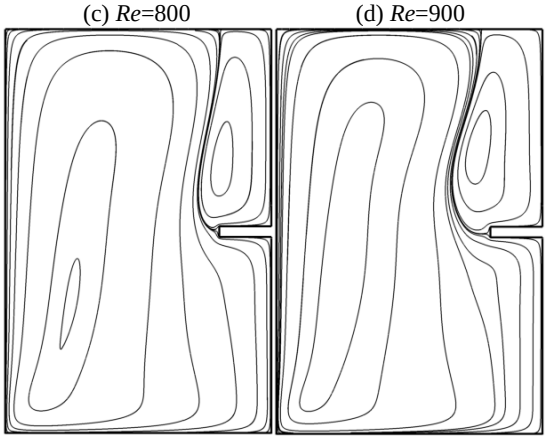

(e) *Re*=1200 (f) *Re*=1600

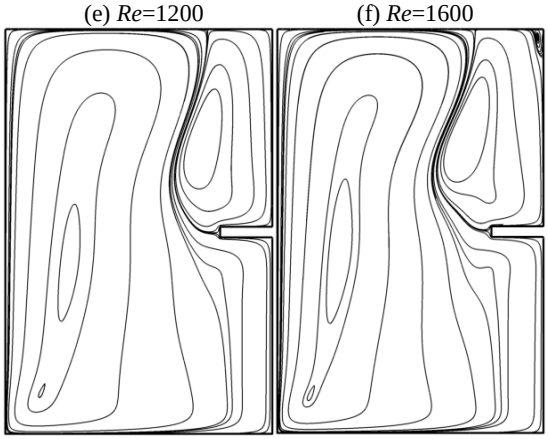

(g) *Re*=1800 (h) *Re*=2100

Figure 4: Evolution of the vortex breakdown flow with Reynolds number for the disk-scaffold, cases as labelled.

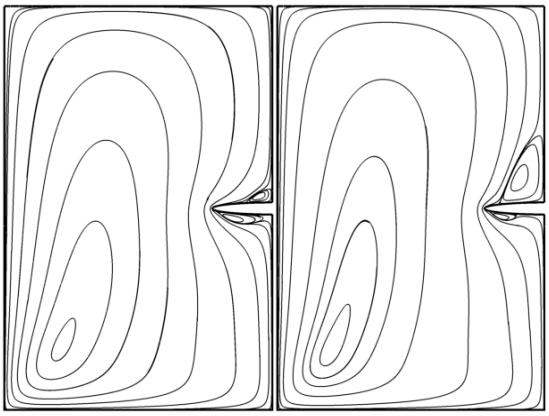

(a) *Re*=600 (b) *Re*=700

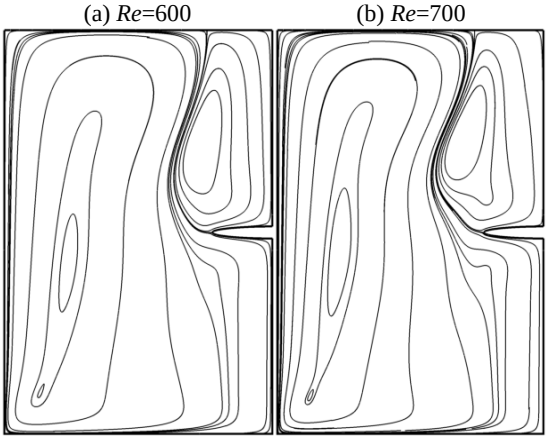

(c) *Re*=1800 (d) *Re*=2100

Figure 5: Selected cases of the vortex breakdown flow for the ellipsoid-scaffold, cases as labelled.

Thus the formation of the recirculation regions referred to as vortex breakdown bubbles. Figure 3 shows the evolution of the VBB as *Re* is increased. Initially appearing on the axis in the interior of the vessel, as *Re* is increased from 800 through to 1000 the bubble volume increases significantly as it expands both axially and radially. At a *Re* just less than 900 the bubble makes contact and merges with the free surface. This connection with the fluid-air interface is expected to provide a pathway for increased oxygen transport to the interior of the vessel, subject of a future investigation. As *Re* is further increased the VBB continues to expand radially around the mid-section, while beginning to contract axially from the lowest point. At *Re*~1800, the streamlines around the left boundary of the VBB have become severely compressed, creating a shear layer of moderate strength between the bubble and the primary cell of fluid; the bubble has reached its greatest radius by this stage and has begun to peel away from the axis at the downstream end. This process continues and is completed by *Re*~2100, at which point the bubble has become completely removed from the cylinder axis and has formed a taurus. This is the final state of the VBB flow in the axisymmetric regime.

Flow States in the presence of an Immersed Body

The sequence of frames in figure 4 shows flow states corresponding to the same *Re* that are shown in figure 3, but for the flow with a disk shaped scaffold–construct present at the axis. With the addition of a body on the cylinder axis there is an early onset of a quasi-VBB state in the form of upstream and distal recirculation zones, adjacent to the upper and lower faces of the disk,

respectively. These zones are already formed at our lowest *Re*=600 case, with the upper bubble initially only extending out to half the disk radius, from the axis, and the lower bubble appearing to envelop the whole underside of the disk. Increasing the *Re* to 700 sees this situation changed, the upstream bubble has expanded considerably both axially and radially and now extends the majority of the way out to the perimeter of the disk, a five-fold increase in size. At the same time the distal bubble has shrunken in size by around 25%, but still covers the majority of the underside of the disk. Neither of these states (*Re*=600 or *Re*=700) are likely conducive to tissue culture due to the non-uniform nature of flow over the construct surface, although the presence of recirculation zones would likely decrease the levels of shear at the scaffold surface due to lower fluid velocities. By *Re*=800 the traditional VBB has developed upstream of the scaffold, with the last remnant of a distal bubble clinging to the underside of the tip. Upon further increase of *Re* the VBB once again begins to expand in the radial and axial directions and attach to the free surface, there is no longer any recirculation zone at the lower surface of the disk. By *Re*~1000 flow has begun to impinge almost normal to the tip of the scaffold (figure 2e for *Re*=1200), this represents an interesting situation, with the direction of flow now uniform from the perimeter to the axis on both upper and lower surfaces of the disk. A flow state such as this could possibly be desirable from a tissue engineering perspective in that it may help to promote uniform growth on both surfaces. This situation continues for the remainder of *Re* considered, with the bubble volume also continuing to increase steadily as the radial expansion continues. The bubble is no longer able to separate from the axis due to the blockage effect of the presence of the disk, and this time the final state has a very large deformed bubble extending from the free surface to the upper face of the scaffold, dominating almost 25% of the area of the meridional semi-plane, with a much smaller, tertiary circulation cell appearing on the cylinder axis, adjacent to the free surface. For reliable assessment of the flow states at higher *Re* than those considered here, three dimensional computations are required. These will be the subject of future investigation, although it is likely that any major increase in *Re* above the present range would not be beneficial to growing tissue.

Modifying the shape of the scaffold to an elliptical profile, while keeping the same volume and length ratios described above, appeared to have little effect on the flow structures observed. Figure 5 shows the flow for the ellipsoid-scaffolds for *Re*=600, 700, 1800, 2100. These include the only Reynolds numbers at which there was a discernable difference in the flow structures observed between the two cases. At *Re*=600 the upper bubble is basically identical to the disk-scaffold case, but the lower bubble is slightly smaller and is not attached to the axis. This bubble is a simple recirculation zone (in the backwards facing step sense) rather than a VBB. With an increase of *Re* to 700 the upper VBB increases in size similarly to the disk-scaffold case but the lower bubble has contracted significantly further. The range $800 \leq Re \leq 1800$ reveals flow patterns almost identical between the two scaffold shapes, as evidenced (for example) by figure 5c. This trend continues until *Re*=2100 where we observe a flow field almost identical to that of the disk-scaffold at the same *Re*, but with no tertiary corner bubble present.

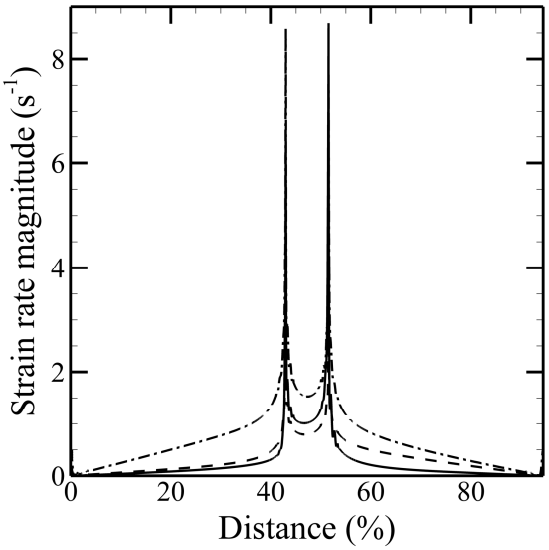

Figure 6: Change in strain rate magnitude over disk-scaffold surface. Distance is in percent of total distance, starting from the point on the axis at the downstream face, ending on the axis at the upstream face. Solid line: *Re*=600, dashed: *Re*=1000, dash-dot: *Re*=2100.

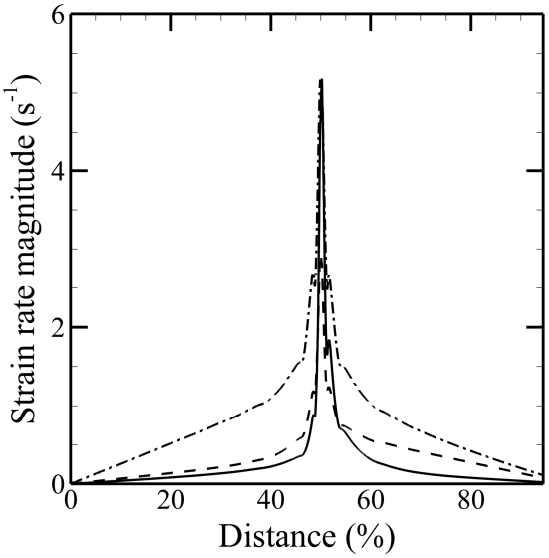

Figure 7: Change in strain rate magnitude over ellipsoid-scaffold surface. Distance and lines as defined in figure 6.

The absence of this tertiary bubble is unlikely to affect the flow field in the vicinity of the scaffold. Figures 6 and 7 allow a more quantitative analysis of the different flow environments experienced by the two different scaffolds. They show the level of strain rate, a direct indicator of shear stress for axisymmetric flows of Newtonian fluids, at the scaffold surface as a function of position around the scaffold perimeter, beginning at the downstream axial location. Three Reynolds numbers are shown for comparison, *Re*=600, 1000, 2100. It is immediately observable that the sharp corners of the disk-scaffold lead to a significant increase in the maximum computed levels of strain and that two localised maxima exist corresponding to the scaffold edges. In general, levels of strain along a given surface (upper or lower) are relatively uniform compared to maximums, particularly at the lower Reynolds numbers. However, there is a slight non-uniformity about the strain rate profiles between the upper

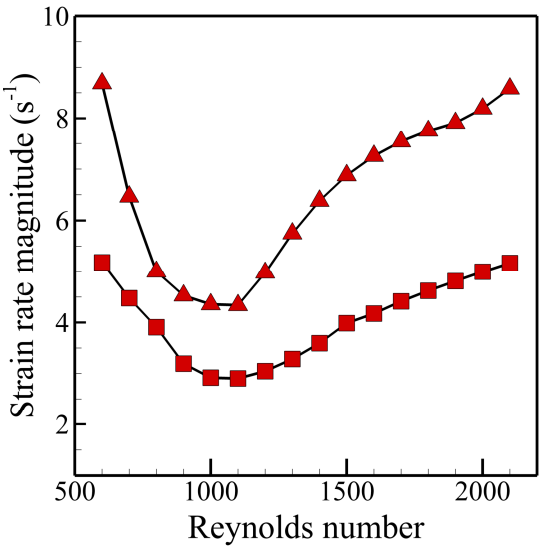

Figure 8: Maximum values of strain rate at scaffold construct surfaces. Triangles: disk-scaffold. Squares: ellipsoid-scaffold.

and lower surfaces for a given scaffold geometry at a given Reynolds number. The severity of this decreases as *Re* is increased, observable by comparing the left hand side of each *Re*=2100 curve to its right hand side. Also worth noting is the fact that the two maximums that exist in the disk-scaffold cases are not of equal magnitude and can vary by up to 31%. This is an undesirable phenomenon when attempting to encourage uniform growth. A pleasing result not directly observable in figures 6 and 7, due to the close proximity of the lines in those plots, is shown in figure 8. The maximum value of strain rate computed at the surface of each construct is plotted with *Re*. It shows that for a significant part of the *Re* range the maximum value of strain rate (and hence shear stress) experienced at a point on the construct surface actually *decreases* with increasing *Re*. This result is somewhat counter-intuitive as an increase in *Re* is usually associated with an increase in velocity throughout the flow field, for a given Newtonian fluid, and hence higher levels of shear stress at no slip surfaces. Certainly of import to the tissue engineering capabilities of a given bioreactor is maximising the mixing and nutrient transport potential while minimising exposure of tissue constructs to harmful levels of fluid forces. The ability to increase the *Re*, thereby possibly increasing the vessel's mixing capability, while at the same time reducing the maximum levels of shear stress acting on immersed bodies may be extremely beneficial. Figure 8 indicates that the present vessel may provide such capabilities over at least the range $600 \leq Re \leq 1100$. Also reinforced by figure 8 is the large decrease in maximum strain between the disk and ellipsoid scaffold shapes, with a drop of up to 65% achievable over the whole *Re* range and drops of approximately 50% achievable for a given *Re*. If nothing else, this would advocate a move away from the disk shaped scaffolds currently employed by the majority of physical researchers in the area of tissue engineering.

CONCLUSION

An investigation into the suitability of a simple base-driven cylinder flow for use in tissue engineering has been performed. Results of the different vortex breakdown flow states observed have been presented and analysed for comparative levels of strain rate (an indicator of shear stress). It is suggested that a range of interim Reynolds numbers, $600 \leq Re \leq 1100$, may provide an ideal regime for tissue culture in these vessels. This was based on the requirement to maximise mass transport and mixing while keeping fluid induced forces to a minimum. Comparison was also made between a common disk shaped scaffold and a rounded ellipsoid scaffold and it was found that the latter may provide improved performance. Fully 3D simulations at slightly higher *Re* may reveal further benefits, and are the focus of ongoing investigation.

ACKNOWLEDGEMENTS

The authors thank the Australian Partnership for Advanced Computing for access to high performance computing facilities. S.J.C. thanks the Department of Mechanical & Aerospace Engineering at Monash University for ongoing financial support.

REFERENCES

BEGLEY C.M. and KLEIS S.J., (2000), "The fluid dynamic and shear environment in the NASA/JSC rotating-wall perfused vessel bioreactor", *Biotech. . Bioeng.*, **70**, 32-40.

DARLING, E.M. & ATHANASIOU, K.A., (2003), "Articular cartilage bioreactors and bioprocesses", *Tissue Engineering*, **9**, 9-26.

DUSTING, J., SHERIDAN, J. & HOURIGAN, K., (2006), "A fluid dynamics approach to bioreactor design for cell and tissue culture", *Biotech. Bioeng.*, **94**, 1196-1208.

HEALEY, J.J., (2007), "Instabilities of flows due to rotating disks: preface", *J. Eng. Math.*, **57** (3), 199-204.

HUSAIN, H.S., SHTERN, V. & HUSSAIN, F., (2003), "Control of vortex breakdown by addition of near-axis swirl", *Phys. Fluids*, **15**, 271-279.

KARNIADAKIS, G., ORSZAG, S. & ISRAELI, M., (1991), "High-order splitting methods for the incompressible Navier-Stokes equations", *J. Comp. Phys.*, **97**, 414-443.

LOPEZ, J.M., MARQUES, F., HIRSA, A.H., & MIRAGHAIE, R., (2004), "Symmetry breaking in free-surface cylinder flows", *J. Fluid Mech.*, **502**, 99-126.

NIKLASON L.E., GAO, J., ABBOTT, W.M., HIRSCHI, K.K., HOUSER, S., MARINI, R. & LANGER, R., (1999), "Functional arteries grown in vitro", *Science*, **284**, 489-493.

SHEARD, G.J. & RYAN, K., (2007), "Pressure-driven flow past spheres moving in a circular tube", *J. Fluid Mech.*, **592**, 233-262.

VUNJAK-NOVAKOVIC, G., (2003) "Fundamentals of tissue engineering: scaffolds and bioreactors", In *Novartis Foundation Symposium*, 34-45. Chichester, New York; John Wiley, 2003.

VUNJAK-NOVAKOVIC, G., FREED, L.E., BIRON, R.J. & LANGER, R., (1996), "Effects of mixing on the composition and morphology of tissue-engineered cartilage", *AIChE Journal*, **42** (3), 850-860.

WOOTTON, D.D. & KU, D.N., (1999), 'Fluid mechanics of vascular systems, diseases and thrombosis", *Ann. Rev. Biomed. Eng.*, **1**, 299-329.